Stable injection locking with slotted Fabry–Perot lasers at 2 μm

JPhys Photonics

OPEN ACCESS

RECEIVED
27 June 2018

REVISED
18 September 2018

ACCEPTED FOR PUBLICATION
5 October 2018

PUBLISHED
6 December 2018

PAPER

Stable injection locking with slotted Fabry–Perot lasers at 2 μm

N Kavanagh[1,2], D Goulding[1,3,4] and F C Garcia Gunning[1,2]

[1] Tyndall National Institute, University College Cork, Ireland
[2] Department of Physics, University College Cork, Ireland
[3] Centre for Advanced Photonics and Process Analysis (CAPPA), Cork Institute of Technology, Ireland
[4] Department of Mathematics, Cork Institute of Technology, Ireland

E-mail: niamh.kavanagh@tyndall.i.e

Keywords: injection-locked lasers, semiconductor lasers, optical communications, optical sensing and sensors

Abstract

Injection locking has many applications in telecommunications systems, such as narrowing linewidths, increasing bandwidth and improving filtering. Beyond telecommunications, injection locking is widely used in remote sensing. This is of particular interest for applications in the 2 μm region, where gases such as carbon dioxide, water vapour and methane have identifiable absorption features. In this paper, we demonstrate stable injection locking with slotted Fabry–Perot lasers in the 2 μm wavelength region. Injection locking was observed in both the optical domain and power spectrum; with key features recorded such as injection 'pulling', side-mode suppression and the characteristic quiet region in the electrical domain denoting single-frequency emission and stable locking. The effect of varying the injection ratio was investigated, with a decreased injection ratio corresponding to a reduction in the locking bandwidth. Finally, the lasers were shown to remain injection locked, with no thermal drift, for over 24 h, indicating their suitability for implementation in a real-world telecommunications system.

1. Introduction

Injection locking (IL) is a powerful technique with wide-ranging applications from communications, through to synchronisation and sensing. Innumerable publications operating at the C-band (1530–1565 nm) have shown the need for IL in phase-sensitive optical amplifiers [1], clock recovery [2], phase recovery [3], filtering [4], bandwidth enhancement [5] and carrier recovery [6] amongst many others. At ~2 μm and mid-IR, however, compact laser availability is limited. This is a waveband of particular interest for gas sensing, where the presence of carbon dioxide (CO_2) at 2004 nm, water vapour (H_2O) at 1854 nm, and even methane (CH_4) at 1654 nm, can be readily detected [7, 8]. The presence of water vapour also makes this waveband important for medical applications [9]. It is relatively easy to find applications utilising quantum cascade lasers (QCLs) in the mid-IR, with IL inevitably used for narrowing their spectral linewidth [10]. However, QCLs predominantly operate in the region beyond 3 μm [11]. It has been shown that extending the band gap of InGaAsP-based devices to ~2 μm is possible, with no re-growth required, and hence availing potential foundry-based, low-cost growth processes [12].

In this paper, for the first time to the best of our knowledge, we are showing stable IL at 2 μm utilising two slotted, multi-quantum well, Fabry–Perot lasers grown on a strained InGaAs/InP platform. IL has been shown to narrow the linewidth of lasers and enable advanced modulation formats at 2 μm [13] and, hence, an understanding of the advantages, challenges and limitations is critical for potential deployment for applications in telecom, remote sensing and biomedical sensing. In section 2, we describe the IL mechanisms, including the expected performance of the lasers, with details of the lasers used in section 3. The IL experimental setup used is typical for IL schemes and is described in section 4. Section 5 contains the results of this experiment and is divided into two subsections: changing the detuning by varying the master laser temperature, while keeping the slave temperature constant and vice versa; varying the slave, while the maser is kept constant, and there are further subsections for increasing and decreasing temperature in each case. We present two different techniques

to observe IL easily: optically, with the aid of an optical spectrum analyser (OSA), and electrically, via direct detection and with the aid of an electrical spectrum analyser (ESA). Stable IL to the main mode was observed, with a maximum IL bandwidth of 6.7 GHz recorded for increasing temperature. A region of single-mode operation (SMO) was also observed around the side mode, with 15 GHz maximum measured. IL hysteresis between increasing and decreasing temperature is also discussed. In section 6, the relationship between the injection ratio and IL bandwidth is investigated. Finally, the lasers were shown to remain injection locked for over 24 h.

2. Principles of IL

The phenomenon of IL occurs when light from one laser (called the master laser, with the main lasing mode centred at the wavelength λ_m or carrier frequency f_m) is injected into the cavity of another laser (called the slave, with the main lasing mode at λ_s or f_s). When the light from the master laser is injected into the slave cavity, the slave laser's internal field will be forced to change from its free-running value.

Within a certain range of f_m values, the master laser can force the slave laser to oscillate at the same frequency as (and at a fixed phase relative to) the master. The width of the locking region is given by a range of values for which the slave laser's frequency is the same as the master's; this is often referred to as the locking range or locking bandwidth. Near this range, f_s is shifted or 'pulled' until it matches f_m, locking the frequencies and maintaining a fixed relative phase between the master and slave [14]. Inside the locking range, it is commonly said that the master has 'captured' the slave and, in this case, if f_m is changed, f_s will follow. This single-frequency emission characterises stable IL. When the detuning (the difference between the main lasing mode of the master laser and main lasing mode of the slave laser, i.e. f_m–f_s) exceeds a certain value, the lasers will unlock and at this point the slave no longer follows the master.

One way to observe IL is to analyse the coupled output of the master and slave lasers, and the effect of the dynamics therein, using an ESA (with the assistance of a photodetector) or an OSA. In the optical domain, IL is identified by injection pulling around the locking range and single-wavelength emission within that range. In the electrical domain, the RF power spectrum requires the use of a square-law detector, which enables a beating peak to be measured at a frequency corresponding to the absolute value of the detuning ($|f_m–f_s|$). As the detuning is reduced, the frequency of this beating peak will decrease to the point at which the laser fields are sufficiently close, so that IL occurs ($f_s = f_m$), and this single-frequency emission corresponds to a 'quiet' region in the RF spectrum, characterising stable IL.

In this paper, we show stable optical IL using two slotted Fabry–Perot lasers operating at ~2 μm wavelength, analysing both the optical and electrical spectra to define the regions of IL.

3. 2 μm master and slave lasers

The availability of lasers emitting at 2 μm is limited, but slotted Fabry–Perot lasers were shown to have performances equivalent to lasers operating at 1.5 μm [12]. Here, our lasers were based on $In_{0.75}Ga_{0.25}As/InP$ multiple-quantum-well slotted Fabry–Perot structures. They were grown on an N-type InP substrate with a P-type InP layer grown on top to form the P-N junction. The active region is composed of InGaAs multiple quantum wells in a separate confinement heterostructure. In order to produce laser emission at wavelengths beyond 1.5 μm, strain was introduced into the active region by increasing the In doping. Straining shifts the band gap to enable emissions at longer wavelengths up to ~2.1 μm [12]. Typically, Fabry–Perot lasers can amplify multiple longitudinal modes simultaneously. In this case, index perturbations in the form of etched features (called slots) were positioned along the laser cavity to manipulate the loss spectrum by enhancing one Fabry–Perot mode and suppressing others, enabling efficient SMO. Essentially, these slots act as a series of smaller Fabry–Perot cavities within the overall cavity, increasing the photon lifetime within the cavity and gradually selecting one mode. This technique of adding index perturbations via slots requires no additional re-growth steps or the use of e-beam lithography, resulting in a cost-effective, and greatly simplified fabrication process for single-mode devices. The lasers were co-packaged with a Peltier element for temperature control [12]. Figure 1(a) shows the free-running optical spectra of the two lasers used in this experiment, with side-mode suppression ratio (SMSR) of ~35 dB for the master laser and ~30 dB for the slave.

Usually, in IL measurements, a tuneable laser source takes the place of the master laser. However, such sources are not widely available at 2 μm, hence it was necessary to tune the operating wavelength of the lasers by adjusting the temperature. Thus, the lasers were fully characterised in terms of thermal tunability and power variation over the range of temperatures used in this experiment; 22.0 °C–42.0 °C for the master laser and 3.5 °C–16.5 °C for the slave laser (in steps of 2.0 °C in each case). These temperature ranges were chosen to ensure that the main mode of each laser could be tuned to overlap with each other in order to investigate the

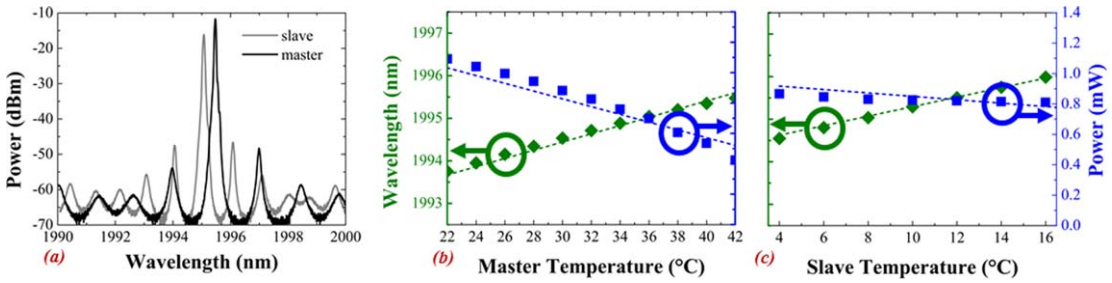

Figure 1. (a) First figure shows the free-running optical spectra of both lasers depicting the master in black with $\lambda_m = 1995.50$ nm (at 41.1 °C, 35 mA, resulting in an SMSR of ~35 dB) and the slave laser in grey with $\lambda_s = 1995.05$ nm (10 °C, 14.3 mA, SMSR = ~30 dB). Next two figures show the laser characterisation of (b) the master laser and (c) the slave laser (both at 60 mA). In (b) and (c) the green data correspond to the left *y*-axis (wavelength in nm) and the blue data with the right y-axis (power in mW), with temperature in °C on the *x*-axis. Points in (b) and (c) show the data collected and the dashed lines represent a linear fit to these data.

Table 1. Linear fit equations of laser characterisation data for wavelength and power with temperature.

Laser	Wavelength—Linear Fit	Adj. R^2
Master	$\lambda = 0.10\ T + 1991.5$	0.9939
Slave	$\lambda = 0.11\ T + 1994.2$	0.9991
Laser	**Power—Linear Fit**	**Adj. R^2**
Master	$P = -0.03\ T + 1.5937$	0.9588
Slave	$P = -0.01\ T + 0.9621$	0.9144

dynamics therein. Both lasers were temperature controlled by a quad-laser driver (ILX LDC 3900), which allows control of four lasers simultaneously, but independently. The temperature stability was assumed to be the same as that of the driver, or $<\pm 0.01$ °C as per specifications. The threshold current for both lasers was ~15 mA at 20 °C (this value was reduced at lower temperatures), with 100 mA maximum operational current for both devices. The current of both lasers was fixed at 60 mA for this characterisation.

The results of the characterisation against temperature are shown in figures 1(b) and (c). In both figures, the green data correspond to the left *y*-axis (wavelength in nm) and the blue data with the right *y*-axis (power in mW), with temperature in °C on the *x*-axis. The points show the data recorded and the dashed lines represent a linear fit to these data, the equations for which are given in table 1.

The adjusted R^2 (Adj. R^2) value indicates how well the terms fit the model. Concerning the variation of the laser wavelength (λ) with temperature (T), the linear fit to these data shows $\Delta\lambda/\Delta T_m = 0.10$ nm °C^{-1} for the master and $\Delta\lambda/\Delta T_s = 0.11$ nm °C^{-1} for the slave, matching the expectations of $\Delta\lambda/\Delta T = 0.1$ nm °C^{-1}, as per [12]. The narrow window of overlap in the region of 1994.50–1995.50 nm can be seen by comparing the green line in both plots.

As first-generation devices, the power of these lasers was low (~1 mW). The variation of the laser power (P) with temperature is shown by the blue data, corresponding to right *y*-axis in figures 1(b) and (c). The blue dashed line represents a linear fit to these data, with $\Delta P/\Delta T_m = -0.03$ mW °C^{-1} for the master and $\Delta P/\Delta T_s = -0.01$ mW °C^{-1} for the slave, indicating that both lasers lose power with increasing temperature. This potential power penalty, the narrow (~1 nm) window of wavelength overlap and limited 0.1 nm °C^{-1} tunability indicate some of the challenges when using these lasers in an IL regime.

4. Experimental setup

The experimental setup is shown in figure 2 and is typical for IL schemes. The fibre-coupled outputs of both lasers were spliced with polarisation controllers (PCs). The polarisation of both lasers was aligned to ensure IL and then not adjusted for the rest of the experiment. An optical circulator (FCIR-2000 N-L-1) was used to couple the light from the master laser into the slave cavity. This circulator had an insertion loss of 1.8 dB (P1 → P2) and 3.8 dB (P2 → P3), providing 16 dB of isolation (P3 → P2 and P2 → P1), measured at 1993 nm. The increased insertion loss from P2 → P3 was due to splicing losses between the fibre from the circulator and the pigtail for connection to the PC. At 2 μm, optical fibre amplifiers in the form of thulium-doped fibre amplifiers (TDFAs)

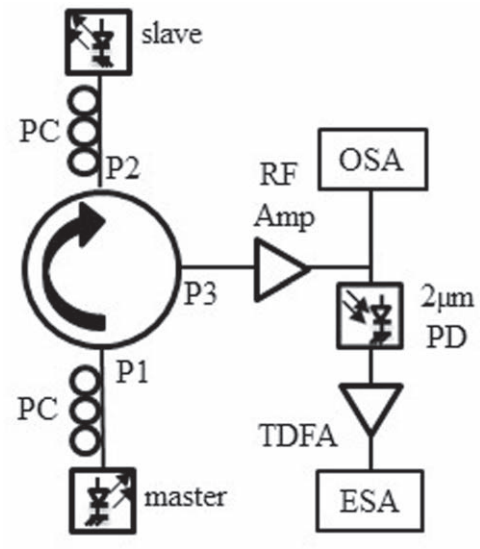

Figure 2. IL setup. Light from the master laser was injected into the slave laser via an optical circulator. The coupled output (amplified with a TDFA) was simultaneously analysed on an ESA (with the aid of a 2 μm PD) and an OSA.

are available and have been shown to operate over a wide band (typically from 1.8–2.10 μm) with gain >35 dB and noise figures as low as 5 dB reported [15]. Thus, to increase the output power of the system, P3 was amplified using a TDFA, prior to detection. The coupled output of the master and slave from P3 was analysed simultaneously on the OSA (Yokogawa AQ6375) and the ESA (Agilient 8565EC). Prior to the ESA, a commercially-available 2 μm InGaAs photodetector (EOT ET-5000F InGaAs PiN detector—PD) with a 3 dB bandwidth of 12.5 GHz was used and, due to the low responsivity of the PD, an electrical amplifier (SHF 804 EA) was added to ensure a reasonable signal-to-noise ratio at the ESA. The bias currents of both lasers were fixed throughout the measurements and both lasers were operated above threshold current to ensure lasing, with the slave biased at 14.3 mA and the master at 35 mA.

5. Experimental IL by tuning wavelengths

Experimental IL investigations with the lasers discussed in section 3 revealed different dynamics depending on which laser is tuned (i.e. master versus slave) and also depending on the direction of tuning towards IL (i.e. decreasing versus increasing). Hence, here in this section, we split the findings between these four different scenarios and analyse potential explanations for the differences observed therein.

5.1. Tuning the master laser

5.1.1. IL by increasing master wavelength while keeping slave constant

The master wavelength was tuned by increasing temperature (T_m) from 22.0 °C to 42.0 °C in steps of 0.1 °C, while the slave temperature (T_s) was kept constant at 10.0 °C, as per figure 1(a), with accuracy as discussed in section 3. The optical spectrum of the coupled output from P3 was recorded at each point.

Figure 3 shows the optical spectra of the coupled output at P3 for three characteristic cases: (a) locking at the side mode, (b) unlocked behaviour and (c) locking at the main mode. In the optical spectrum, IL behaviour is indicated by SMO and an SMSR improvement of ~3 dB from the unlocked to locked states.

Figure 4(a) shows a false colourplot combination of all the optical spectra from each 0.1 °C measurement. We can see that increasing master temperature on the *x*-axis corresponds linearly to increasing master wavelength on the *y*-axis, as expected. The slave wavelength was fixed at $\lambda_s = 1995.05$ nm throughout. The relative intensity of the peaks is denoted by the colour bar on the right, with red indicating more intense optical power and blue representing less intensity.

Looking from left to right in figure 4(a), IL of the slave laser to the master can be seen when the main lasing mode of the master overlaps with the **side mode** of the slave laser at 1994.05 nm. Within this range, the slave's main mode is suppressed and lasing occurs at λ_m only. This region of SMO can be observed from $T_m = 25.2$ °C– 27.2 °C. The master laser has captured the slave and when λ_m is changed, λ_s follows. The combined injected peak at $\lambda_s = \lambda_m$ is of greater intensity than the previous slave or master peaks. It can also be seen that the side-modes of the slave laser are suppressed and following the master laser, demonstrating that IL

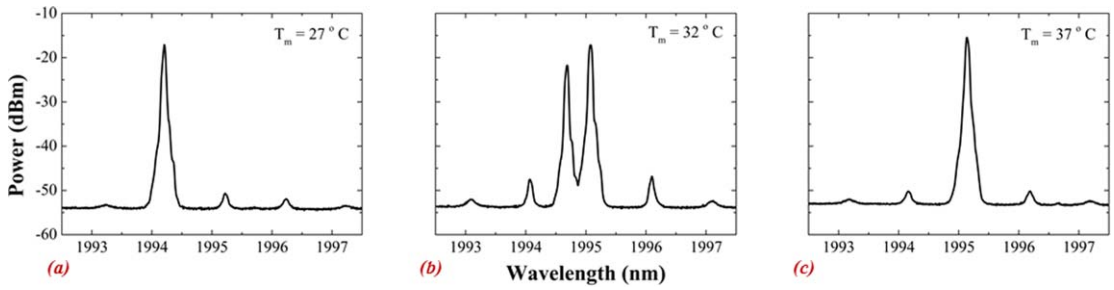

Figure 3. Optical spectra depicting the coupled output of the slave laser, at 10 °C, and the master, with temperature T_m. Three characteristic regions are shown: (a) locking at the side mode, (b) unlocked with master main mode at 1994. 70 nm, slave main mode at 1995.05 nm and side-modes at ∼1994 nm, 1996 nm; (c) locking at the slave's main mode. Suppression of other cavity modes between the unlocked/locked states can be seen.

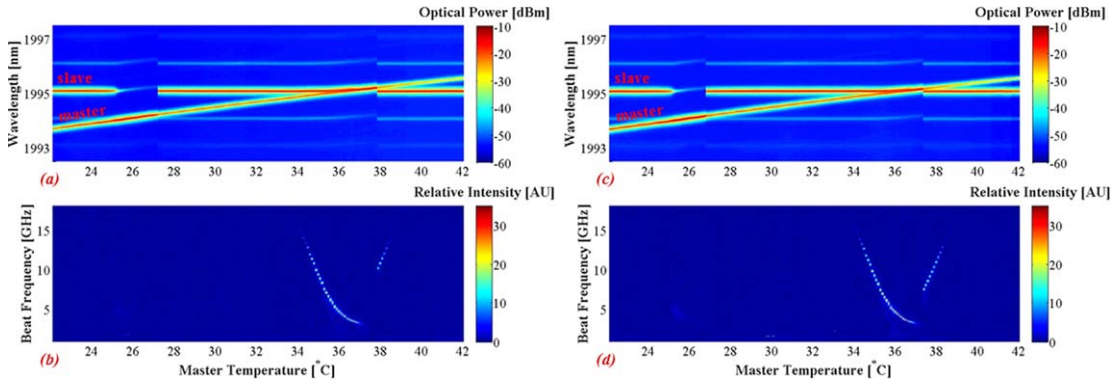

Figure 4. OSA data above, ESA data below, for increasing master temperature on the left side and decreasing master temperature on the right side (with the slave temperature fixed in both cases). SMO around the side mode can clearly be seen in the OSA data above and IL to the main mode is signified by the characteristic quiet region in the ESA data, beating peak curve, below.

affects the laser cavity as a whole. Outside the locking region, at $T_m = 27.2$ °C, the slave laser unlocks, with lasing returning to the slave's main mode at $\lambda_s = 1995.05$ nm and the slave no longer following the master.

As the master moves towards the **main** mode of the slave laser in figure 4(a), the effects of IL can be observed around 35.9 °C–37.8 °C. Again, suppression and pulling of the side-modes can be seen, the slave laser follows the master and the injected peak is of greater intensity. At 37.8 °C the unlocking boundary is very clear in the optical domain. Note that around the locking boundary, the separate slave and master laser peaks may not be distinguishable due to the limited resolution of the OSA, which was 0.05 nm (or 3.75 GHz at 2 μm), therefore making the determination of the locking/unlocking regions difficult. Hence, it was decided that a more accurate measurement to verify IL would be to utilise the ESA.

Thus, while the optical spectrum of the coupled output from P3 was recorded at each $\Delta T_m = 0.1$ °C point from 22.0 °C–42.0 °C, the power spectrum was acquired simultaneously. 'Max Hold' averaging for 30 s was used before saving the ESA trace at each point, to ensure acquisition of a beating tone. Upon analysis of these data, it was found that the noise floor of the power spectrum was significantly slanted towards lower frequencies, which made determining the beating peak difficult, especially as the detuning reduced to zero. In order to combat this, the experiment was repeated with the lasers switched off to isolate the noise data. These noise data was then subtracted from the experimental data, producing a power spectrum with a flat noise floor from which the beating peak could clearly be distinguished. Figure 4(b) shows a false colourplot combination of all these power spectra, with the beating frequency on the *y*-axis and the temperature of the master laser on the *x*-axis, again the slave laser was fixed at 10.0 °C.

Looking from left to right, moving towards the **side mode** of the slave laser, no beating peaks were detected around the locking region at $T_m = 25.2$ °C–27.2 °C. This is due to the limited 3 dB bandwidth of 12.5 GHz of the 2 μm PD used with the ESA. 12.5 GHz corresponds to 0.17 nm at 2 μm. Therefore, since the detuning between the slave and laser peaks was >0.17 nm around this locking range, beating peaks were not recorded in this region. As the master was tuned towards the **main** mode of the slave laser, the detuning was reduced to within the bandwidth of the detector and a beating peak was detected in figure 4(b). Initially, the frequency of this beating peak reduced linearly towards zero with increasing master temperature, as per

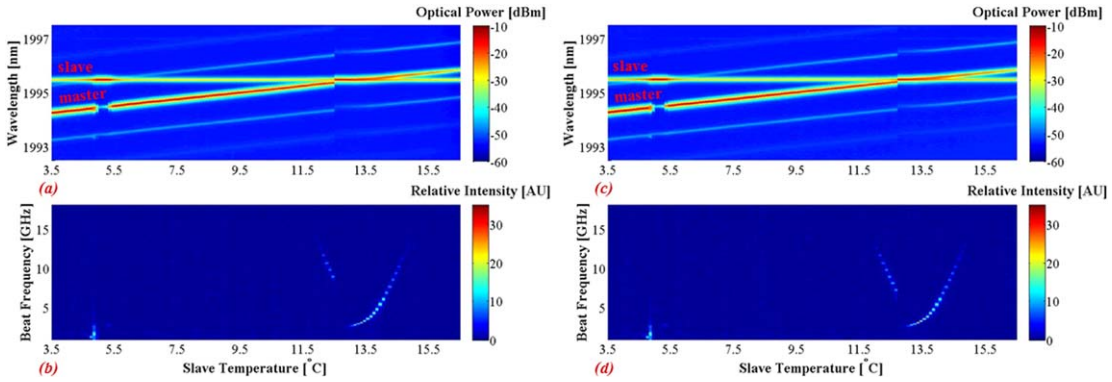

Figure 5. OSA data above, ESA data below, for decreasing slave temperature on the left side and increasing slave temperature on the right side (with the master temperature fixed in both cases). Figures 5(a)–(d) can be compared to the corresponding plots in figures 4(a)–(d), as the detuning is varied similarly in each case. Notably, the ESA beating peak curve is flipped by 180° for example.

$\Delta\lambda/\Delta T = 0.1$ nm °C^{-1}. However, near the locking region, the relationship no longer followed the linear pattern and the effect of the master laser 'pulling' the slave could be seen. When the laser fields were sufficiently close, single-frequency emission was observed ($f_s = f_m$) and no beating peak was recorded on the ESA between $T_m = 36.9$ °C–37.8 °C. Thus, stable IL was observed, with no other frequencies recorded in this region. When the master laser was tuned beyond the locking region, the beating peak returned and its frequency once again increased linearly with increasing temperature.

5.1.2. IL by decreasing the master wavelength while keeping the slave constant

The same experiment was repeated for decreasing master temperature. The region of SMO at the side mode and IL bandwidth at the main mode was calculated by converting the width in temperature (for example $T_m = 25.2$ °C to 27.2 °C is 2 °C width) to wavelength (in nm) using the $\Delta\lambda/\Delta T$ characterisation from table 1 and then converting this to frequency using the relation

$$\frac{\Delta\lambda}{\Delta\nu} = \frac{\lambda^2}{c},$$

where $\Delta\lambda$ = wavelength range, $\Delta\nu$ = frequency range, c = speed of light and $\lambda = 2$ μm. The error value was taken as the temperature step (0.1 °C) and this was converted in the same way.

Similar results were observed in figures 4(c) and (d) with the notable difference that, for decreasing T_m, the region of SMO at the slave's side mode was (12.0 ± 0.7) GHz, compared to (15.0 ± 0.7) GHz for increasing T_m. Similarly, the stable IL bandwidth at the main mode was (3.7 ± 0.7) GHz for decreasing T_m, compared to (6.7 ± 0.7) GHz for increasing T_m. This hysteresis is typical in IL schemes, given that the carrier density dependent refractive index strongly affects the IL of semiconductor lasers, resulting in asymmetric tuning characteristics [16, 17].

5.2. Tuning the slave laser

5.2.1. IL by decreasing the slave wavelength and keeping the master constant

In order to implement IL as a filtering mechanism in a dense wavelength division multiplexing (DWDM) telecommunications system, it would be necessary to tune the slave rather than the master. In such a scenario, the receiver would incorporate a slave laser and would tune to the incoming DWDM master signal. Thus, a reversal of the above experiment was performed, this time adjusting the slave laser, while keeping the master constant. In this way, the slave wavelength was tuned by decreasing temperature from 16.5 °C to 3.5 °C in steps of 0.1 °C, while the master temperature was kept constant, as per figure 1(a), at 41.1 °C ($\lambda_m = 1995.50$ nm), with accuracy as discussed section 3.

The resulting OSA spectrum can be seen in figure 5(a). In practical terms, this section—decreasing the slave wavelength (from 1995.90 nm), while holding the master constant (at 1995.50 nm) figure 5(a), can be compared to section 5.1.1—increasing the master (from 1993.70 nm), while keeping the slave fixed (at 1995.05 nm) figure 4(a), as both methods change the detuning in the same fashion.

However, when comparing the figures for increasing master temperature in figure 4 to those for decreasing slave temperature in figure 5, some differences can be seen. In figure 5(a) the effects of IL the slave laser to the master can be observed from $T_s = 4.9$ °C–5.3 °C when the side mode of the slave overlaps with the main mode of the master laser. The region of SMO is significantly reduced to (3.0 ± 0.7) GHz in comparison to (15.0 ± 0.7) GHz in figure 4(a). We believe that this decrease (in the case of decreasing slave temperature, compared to

Table 2. Summary of the results from the four IL scenarios depending on increasing/decreasing temperature of the master/slave laser (T_m/T_s). The width of the SMO region at the side mode (SM) and IL bandwidth main mode (MM) is given in GHz for each case.

T_m	T_s	SMO SM (GHz)	IL MM (GHz)
Increased	Fixed	15.0 ± 0.7	6.7 ± 0.7
Decreased	Fixed	12.0 ± 0.7	3.7 ± 0.7
Fixed	Decreased	3.0 ± 0.7	4.5 ± 0.7
Fixed	Increased	3.0 ± 0.7	3.0 ± 0.7

increasing master temperature in section 5.1.1) may be due to a reduction in the injection ratio. The master laser has a higher power penalty with increasing temperature ($\Delta P/\Delta T_m = -0.03$ mW °C^{-1}) in comparison to the slave laser ($\Delta P/\Delta T_s = -0.01$ mW °C^{-1}), as per section 3. Therefore, the injection ratio for the range in this section: $T_s = 16.5$ °C → 3.5 °C with $T_m = 41.1$ °C would likely be lower compared to the range in section 5.1.1: $T_m = 22.0$ °C → 42.0 °C with $T_s = 10.0$ °C. This relation between the injection ratio and IL is investigated in further detail in section 6.

In figure 5(b), high-intensity features are observed in the power spectrum of the laser, corresponding to non-linear dynamical behaviour close to the IL boundary of the lower wavelength side mode. These non-linear dynamical features lie outside the scope of the current paper. A notable difference between figures 4(b) and 5(b) is the shape of the ESA beating peak curve. However, this beating peak curve for decreasing slave temperature can be mapped almost exactly onto the beating peak curve for increasing master temperature if flipped by 180 degrees. Thus, in the case of tuning the slave, while fixing the master (versus tuning the master, while fixing the slave), the beating dynamics are similar but the regions of linearity and injection 'pulling' are reversed.

5.2.2. IL by increasing the slave wavelength and keeping the master constant

Finally, the slave wavelength was increased from 1994.30 nm, while holding the master constant at 1995.50 nm, figures 5(c) and (d), which in turn can be compared to section 5.1.2—decreasing the master from 1995.60 nm, while keeping the slave fixed at 1995.05 nm, figures 4(c) and (d). Previously, decreasing the master wavelength to reduce detuning resulted in a reduction in the IL bandwidth (in comparison to increasing master wavelength). Less narrowing was seen here, with the region of SMO at the side mode the same in each case, (3.0 ± 0.7) GHz for both increasing and decreasing T_s. However, slight narrowing in the IL bandwidth was recorded at the main mode with (4.5 ± 0.7) GHz for decreasing T_s and (3.0 ± 0.7) for increasing T_s. This further demonstrates that when tuning the slave rather than the master, the injection dynamics are similar but reversed.

5.3. Analysis

Table 2 summarises the results from the four IL scenarios depending on increasing/decreasing temperature for the master or the slave laser (T_m/T_s). The width of the SMO at the side mode and IL bandwidth at the main mode is given in GHz for each case. This summary again shows that, due to the low flexibility of operating conditions of the two lasers, the IL bandwidth is compromised when the slave is tuned to the master rather than vice versa. Nevertheless, stable locking is observed in all cases.

6. Further IL experimental analyses

6.1. Injection ratio

In section 5.2.1, it was discussed that the observed decrease in IL bandwidth (when tuning the slave versus tuning the master in section 5.1.1) may be due to a reduction in the injection ratio. For this reason, the relation between the injection ratio and IL bandwidth was investigated in further detail. Typically, the IL bandwidth will increase if the ratio of injected master power to slave power (called the injection ratio) is increased [18, 19]. However, in the experiments performed here, the master laser was tuned to higher temperatures (around 40 °C) in the region of overlap compared to the slave laser (around 10 °C) within this window, which meant that the slave laser presented higher power, since both lasers suffered power penalty with increasing temperature, as per figure 1. For this reason, it was difficult to obtain an injection ratio >0 dB, where the master was more powerful than the slave laser. Therefore, as a proof of principle, increasingly negative injection ratios were investigated. In this way, one would expect that as the injection ratio is decreased, the IL bandwidth should also decrease.

As mentioned, the injection ratio is defined as the ratio between the injected power from the master laser and the optical power of the free-running slave laser. However, as an initial investigation in this case, the injection ratio was taken as the ratio of the master laser peak power to the slave laser peak power at 1 nm distance apart on

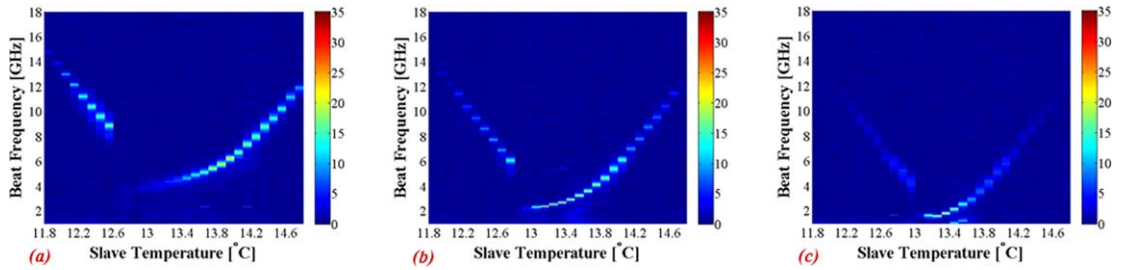

Figure 6. ESA data for decreasing injection ratios from left to right: (a)—3 dB, (b)—10 dB, (c)—17 dB indicating that reduced injection ratio correspond to decreasing IL bandwidth. Colour bar on the right indicates the relative intensity (in arbitrary units) for all three plots.

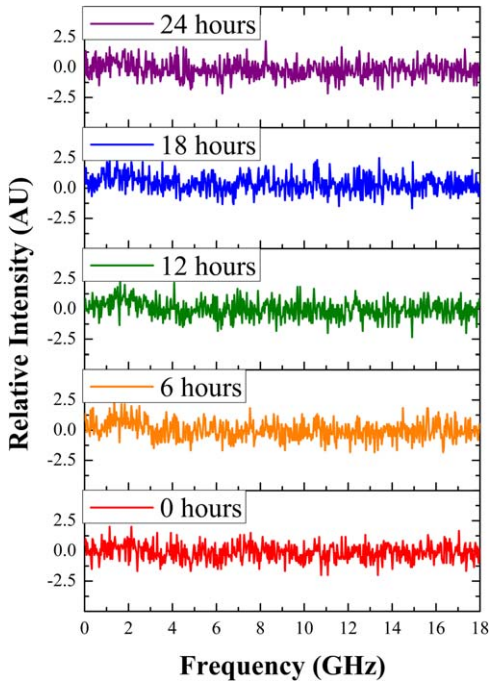

Figure 7. Results of stability test showing snapshots of the relative intensity versus frequency from the ESA data, in 6 h intervals. No distinctive beating peaks were recorded for over 24 h, indicating that the lasers remained locked for that time.

Table 3. Summary of the results showing the relation between the injection ratio and IL bandwidth (BW).

Ratio (dB)	IL BW (GHz)
−3	2.2 ± 0.7
−10	1.5 ± 0.7
−17	0.7 ± 0.7

the coupled optical spectrum, with the slave wavelength then increased and swept across the region of the master's (fixed) main mode as before. Using this method, three distinct injection ratio measurements were made with values of approximately −3, −10 and −17 dB. As can be seen from figure 6, reducing the ratio of the master power to the slave power did result in a reduction in the stable locking range, indicated by the narrowing quiet region in the ESA data. The minimum injection ratio measured was −17 dB approx. because below that the margin of error became too large. A smaller temperature increment would be needed for a more accurate measurement beyond this point. Nonetheless, a trend was established and the summarised findings are depicted in table 3.

6.2. Stability over time

Finally, if this IL technique were to be implemented in a DWDM transmission system, the lasers must remain locked, and not display thermal drift, over long periods of time to ensure error-free performance.

To test suitability for this, IL was achieved (by decreasing T_s to 12.8 °C, while T_m was fixed at 41.1 °C) and an automatic peak search of the ESA data was performed every 30 s for over 24 h. The peak search was performed after the noise floor was subtracted from the active data and the minimum threshold was set to 4 GHz, as this was the approximate minimum beating peak recorded in previous measurements.

Figure 7 shows several snapshots of the data acquisition in 6 h intervals. No beating peaks were detected over 24 h, thus the lasers remained locked. It was notable that no mode-hopping was observed over the course of all measurements. By comparing the optical spectra at the start and end of this measurement, it was also found that the lasing peak of the injection-locked lasers did not display any thermal drift over the time period, further indicating the suitability of these lasers for potential implementation in an optical communications system.

7. Conclusion

In this paper, we have presented, for the first time to the best of our knowledge, a comprehensive study of stable IL in the 2 μm wavelength region utilising slotted InGaAs/InP Fabry–Perot lasers. Common characteristics of IL were observed in both the optical domain and RF power spectrum, such as injection 'pulling', side-mode suppression and the distinctive quiet region in the electrical domain denoting single-frequency emission and stable locking. Two locking regions were observed in each case; a region of SMO around the side mode and stable IL at the main mode. A maximum stable IL bandwidth of 6.7 GHz was measured at the main mode for increasing master temperature, with a region of SMO of 15 GHz measured around the side mode in this case. These figures were reduced to 3.7 and 12 GHz, respectively, for decreasing master temperature, thus displaying the theoretically predicted IL hysteresis. In addition, as expected in IL systems, it was found that decreasing the injection ratio (from −3 to −17 dB, for example) corresponded to a reduction in the locking bandwidth (from 2.2 to 0.7 GHz, respectively). Finally, the lasers were shown to remain injection locked, with no thermal drift, for over 24 h, indicating their suitability for implementation in a real-world telecommunications system. We believe this IL demonstration illustrates the growth in key enabling technologies at 2 μm and presents exciting opportunities for future applications in this new waveband.

Acknowledgments

The authors would like to acknowledge equipment support from Eblana Photonics. Thanks are also extended to Padraic Morrissey and Brian Corbett (Tyndall) for helpful discussions. We would like to acknowledge funding support from the Irish Research Council (GOIPG/2014/637), Science Foundation Ireland under IPIC (12/RC/2276) and (13/CDA/2103), and EU FP7 IP project MODEGAP (258033).

ORCID iDs

N Kavanagh https://orcid.org/0000-0003-0791-3964
F C Garcia Gunning https://orcid.org/0000-0003-3468-5813

References

[1] Slavík R *et al* 2010 All-optical phase and amplitude regenerator for next-generation telecommunications systems *Nat. Photon.* **4** 690
[2] Mathason B K and Delfyett P J 2000 Pulsed injection locking dynamics of passively mode-locked external-cavity semiconductor laser systems for all-optical clock recovery *J. Lightwave Technol.* **18** 1111
[3] Slavík R, Liu Z and Richardson D J 2017 Optical injection locking for carrier phase recovery and regeneration *Optical Fiber Communication Conf.* paper Th4I.3
[4] Cotter W, Goulding D, Roycroft B, O'Callaghan J, Corbett B and Peters F H 2012 Investigation of active filter using injection-locked slotted Fabry–Perot semiconductor laser *Appl. Opt.* **51** 7357–61
[5] Jin X and Chuang S L 2006 Bandwidth enhancement of Fabry–Perot quantum-well lasers by injection-locking *Solid-State Electron.* **50** 1141–9
[6] Liu Z, Kim J Y, Wu D S, Richardson D J and Slavík R 2015 Homodyne OFDM with optical injection locking for carrier recovery *J. Lightwave Technol.* **33** 34–41
[7] Cariou J P, Augere B and Valla M 2006 Laser source requirements for coherent lidars based on fiber technology *Compt. Rend. Phys.* **7** 213–23
[8] Khan A, Schaefer D, Tao L, Miller D J, Sun K, Zondlo M A, Harrison W A, Roscoe B and Lary D J 2012 Low power greenhouse gas sensors for unmanned aerial vehicles *Remote Sens.* **4** 1355
[9] Alexeeva N and Arnold M 2009 Near-infrared microspectroscopic analysis of rat skin tissue heterogeneity in relation to noninvasive glucose sensing *J. Diabetes Sci. Technol.* **3** 219

[10] Taubman M, Myers T, Cannon B and Williams R 2004 Stabilization, injection and control of quantum cascade lasers, and their application to chemical sensing in the infrared *Spectrochim. Acta* A **60** 3457–68
[11] Vitiello M S, Scalari G, Williams B and De Natale P D 2015 Quantum cascade lasers: 20 years of challenges *Opt. Express* **23** 5167–82
[12] Phelan R, O'Carroll J, Byrne D, Herbert C, Somers J and Kelly B 2012 $In_{0.75}Ga_{0.25}As/InP$ multiple quantum-well discrete-mode laser diode emitting at 2 μm *IEEE Photonics Technol. Lett.* **24** 652–4
[13] Liu Z *et al* 2014 Up to 64QAM (30 Gbit/s) directly-modulated and directly detected OFDM at 2 μm wavelength *40th European Conf. on Optical Communications*
[14] Lau E, Wong L and Wu M 2009 Enhanced modulation characteristics of optical injection-locked lasers: a tutorial *IEEE J. Sel. Top. Quantum Electron.* **15** 618–33
[15] Li Z, Heidt A M, Daniel O, Jung J M, Alam Y and Richardson DJ S U 2013 *Opt. Express* **21** 9289–97
[16] Kobayashi K, Nishimoto H and Lang R 1982 Experimental observation of asymmetric detuning characteristics in semiconductor laser injection locking *Electron. Lett.* **18** 54–6
[17] Guo P, Yang W, Parekh D, Chang-Hasnain C J, Xu A and Chen Z 2013 Experimental and theoretical study of wide hysteresis cycles in 1550 nm VCSELs under optical injection *Opt. Express* **21** 3125–32
[18] Bogris A, Syvridis D, Fragkos A, Nikas T, Simos H and Elsäßer W 2016 Optical injection in semiconductor lasers: physics and applications *18th Int. Conf. on Transparent Optical Networks*
[19] Daly A, Roycroft B and Corbett B 2013 Stable locking phase limits of optically injected semiconductor lasers *Opt. Express* **21** 30126–39